

the catalyst. In this case the oxidative dissolution of Pt(O) is the limiting factor in the stability and long-term use of n-MS₂/Pt photoanodes for Cl₂ generation. Active research is being pursued in our labs toward development of durable catalyst coatings for n-type semiconductors for Cl₂ and O₂ generation. The ideal catalyst coating will have to show stability toward oxidation and/or attack by Cl⁻, OH⁻, Cl₂, and O₂ and possibly enable the use of n-type semiconductors in less concentrated electrolyte solutions.

Acknowledgment. We thank the United States Department of Energy, Office of Basic Energy Sciences, Division of Chemical Sciences, and GTE Laboratories for support of this work. A.J.R. acknowledges support as an

M.I.T. NPW Fellow, 1982-1983, and D.J.H. acknowledges support for graduate study from NSERC of Canada. Use of the Central Facilities of the Center for Materials Science and Engineering is gratefully acknowledged.

Registry No. MoS₂, 1317-33-5; WS₂, 12138-09-9; Pt, 7440-06-4; Cl⁻, 16887-00-6; Br⁻, 24959-67-9.

Supplementary Material Available: Three tables giving output parameters for a variety of platinized n-WS₂ and n-MoS₂ photoanode-based cells in aqueous Cl₂/LiCl and Br₂/LiBr, and in CH₃CN/Cl₂/Cl⁻ and CH₃CN/Br₂/Br⁻ (4 pages). Ordering information is given on any current masthead page.

Quadrupole Echo Study of Internal Motions in Polycrystalline Media

Leslie J. Schwartz,[†] Eva Meirovitch,^{†‡} John A. Ripmeester,[§] and Jack H. Freed^{*†}

Baker Laboratory of Chemistry, Cornell University, Ithaca, New York 14853; Isotope Department, Weizmann Institute of Science, Rehovot 76 000 Israel; and National Research Council of Canada, Division of Chemistry, Ottawa, Ontario, Canada K1A 0R9 (Received: February 23, 1983; In Final Form: June 7, 1983)

Quadrupole echo spectra of polycrystalline trimethylsulphoxonium-*d*₉ iodide (TMSI-*d*₉) and hexamethylbenzene-*d*₁₈ (HMB-*d*₁₈) in the slow- and fast-motional temperature regions are analyzed via a dynamic line-shape formalism which incorporates the stochastic Liouville operator. Both molecules are found to exhibit two approximately independent motional modes: methyl-group rotation, and discrete jumps about a single axis. For TMSI-*d*₉, this latter mode consists of 3-fold jumps about an axis tilted $67.5 \pm 1.0^\circ$ with respect to the S-C axis, with an activation energy $E_A = 11.1 \pm 0.9$ kcal/mol and an inverse frequency factor $\tau_0 \approx 6 \times 10^{-13}$ s, while HMB-*d*₁₈ reorients about its hexad axis with $E_A = 5.3 \pm 0.2$ kcal/mol and $\tau_0 \approx 2 \times 10^{-12}$ s. Simulations based on the Fourier transforms of calculated free induction decays (instead of calculated echoes) are inadequate for much of the temperature ranges studied.

I. Introduction

The development of solid-state NMR techniques¹ has made it possible to obtain well-resolved NMR line shapes from polycrystalline materials. Contrary to liquids, where rapid molecular reorientation can effectively average out any effects that slow, anisotropic internal motions have on the spectra, in solids, internal motions (involving molecular segments rather than entire molecules) can be the only ones present. Changes in NMR line shapes will result when the rates of the internal dynamic processes are on the NMR time scale.

For many years, dynamic processes in solids were followed by dielectric relaxation, broad-line NMR, and spin-lattice relaxation measurements.² In many instances, the exact dynamic model presented in such NMR studies depended on second moment calculations based on crystal structure data, assumed structural features, and likely models for the motion.

More recently, with the advent of multiple-pulse, cross-polarization, and dipolar decoupling techniques,¹ the ability to obtain well-resolved NMR spectra of spin $1/2$ nuclei has led to the development of complete dynamic line-shape formulations³⁻⁵ which can yield very specific information on both motional models and rates.

For spin 1 nuclei (such as ²H) with large quadrupole splittings, it is impossible to obtain the NMR line shape

directly by Fourier transformation of the free induction decay (fid), as it is impossible to detect an undistorted fid within a few microseconds of the rf pulse. In this instance, the quadrupole echo sequence⁶ may be used to refocus the magnetization and the line shape can be obtained by Fourier transformation of the half-echo.

In the presence of slow motions, ²H spectra obtained from quadrupole echoes may differ significantly from those expected from the fid⁷ because of irreversible dephasing during the echo pulse separation time. However, line shapes obtained from quadrupole echoes in the slow-motional region can still give quite specific information on motional models and rates, provided that unavoidable experimental distortions are properly accounted for. For

(1) (a) A. Pines, M. G. Gibby, and J. S. Waugh, *J. Chem. Phys.*, **59**, 569 (1973); (b) U. Haebleren, *Adv. Magn. Reson.*, **S1** (1976); (c) M. Mehring in "NMR: Basic Principles and Progress", Vol. 11, P. Diehl, E. Fluck, and R. Kosfeld, Eds., Springer-Verlag, New York, 1976.

(2) P. S. Allen, *Phys. Chem. (MTP)*, **4**, 43 (1972).

(3) D. E. Wemmer, Ph.D. Thesis, University of California, Berkeley, CA, 1978; see also ref 1c, p 39.

(4) H. W. Spiess in "NMR: Basic Principles and Progress", Vol. 15, P. Diehl, E. Fluck, and R. Kosfeld, Eds., Springer-Verlag, New York, 1978, and references cited within.

(5) R. F. Campbell, E. Meirovitch, and J. H. Freed, *J. Phys. Chem.*, **83**, 525 (1979).

(6) (a) I. Solomon, *Phys. Rev.*, **110**, 61 (1958); (b) J. H. Davis, K. R. Jeffrey, M. Bloom, M. I. Valic, and T. P. Higgs, *Chem. Phys. Lett.*, **42**, 390 (1976).

(7) (a) H. W. Spiess and H. Sillescu, *J. Magn. Reson.*, **42**, 381 (1981); (b) D. E. Woessner, B. S. Snowden, Jr., and G. H. Meyer, *J. Chem. Phys.*, **51**, 2968 (1969).

[†]Cornell University.

[‡]Weizmann Institute of Science.

[§]NRC of Canada.

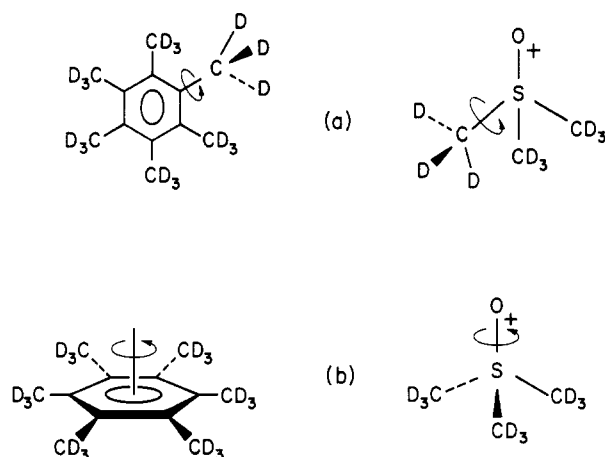
Hexamethylbenzene- d_{18} Trimethylsulphoxonium- d_9 iodide

Figure 1. Two idealized independent internal motional modes of hexamethylbenzene- d_{18} and trimethylsulphoxonium- d_9 iodide: (a) methyl-group rotation; (b) interchange of methyl groups.

example, in previous studies of deuterated phospholipids and other biochemically interesting molecules, workers have successfully used finite site jump models to describe the dynamics of these systems under the quadrupole echo sequence.^{8,9}

Presented in this report are experimental and simulated quadrupole echo spectra for two deuterated polycrystalline materials: trimethylsulphoxonium- d_9 iodide (TMSI- d_9) and hexamethylbenzene- d_{18} (HMB- d_{18}). We find that both of these molecules experience two independent internal motional modes, as shown in Figure 1. With an increase in temperature from the true rigid limit, the individual methyl groups begin rotating, and the NMR line shapes change with temperature until they are motionally averaged with respect to deuterium interchange, although still in the rigid limit with respect to other motions. The methyl groups themselves then begin interchanging positions, and the spectra go through dramatic changes until they once again reach a motionally narrowed limit.

In past studies on HMB- d_{18} ¹⁰ and TMSI¹¹ based upon T_1 , $T_{1\rho}$, and second moment analyses, the results were also interpreted in terms of rapid methyl-group rotation and slower overall rotation about the molecular symmetry axis. For HMB^{3,12-14} there has been a ^{13}C line-shape analysis³ as well. We emphasize in the present work how full line-shape analysis leads to unequivocal assignment of the two types of molecular motion and how in favorable cases one can discriminate between different motional models. We also compare our results with previous measurements, and we comment on isotope effects on the motions of the deuterated vs. protonated molecules.

Our formulation for calculating spin echoes uses the stochastic Liouville equation to govern the time dependence of the density matrix between pulses and idealizes the effects of the pulses as rotations of the density matrix.

(8) D. M. Rice, R. J. Wittebort, R. G. Griffin, E. Meirovitch, E. R. Stimson, Y. C. Meinwald, J. H. Freed, and H. A. Scheraga, *J. Am. Chem. Soc.*, **103**, 7707 (1981).

(9) (a) A. Blume, D. M. Rice, R. J. Wittebort, and R. G. Griffin, *Biochemistry*, **24**, 6220 (1982); (b) A. Blume and R. G. Griffin, *ibid.*, **24**, 6230 (1982); (c) A. Blume, R. J. Wittebort, S. K. Das Gupta, and R. G. Griffin, *ibid.*, **24**, 6243 (1982). (See also references cited in these works.)

(10) J. Tang, L. Sterna, and A. Pines, *J. Magn. Reson.*, **41**, 389 (1980).

(11) S. Jurga, K. Jurga, and Z. Pajak, *J. Phys. Chem.: Solid State Phys.*, **14**, 4433 (1981).

(12) P. S. Allen and A. Cowking, *J. Chem. Phys.*, **47**, 4286 (1967).

(13) D. Suwelack, W. P. Rothwell, and J. S. Waugh, *J. Chem. Phys.*, **73**, 2559 (1980), and references cited within.

(14) W. P. Rothwell and J. S. Waugh, *J. Chem. Phys.*, **74**, 2721 (1981).

TABLE I: Irreducible Spherical Tensor Angular Momentum Operator Basis Set^a

tensor	operator form	matrix elements ^b
\hat{T}_{00}	$3^{-1/2}\hat{I}$	$3^{-1/2}\begin{pmatrix} 1 & 0 & 0 \\ 0 & 1 & 0 \\ 0 & 0 & 1 \end{pmatrix}$
\hat{T}_{11}	$-2^{-1/2}\hat{I}$	$\begin{pmatrix} 0 & -1 & 0 \\ 0 & 0 & -1 \\ 0 & 0 & 0 \end{pmatrix}$
\hat{T}_{10}	\hat{I}_z	$\begin{pmatrix} 1 & 0 & 0 \\ 0 & 0 & 0 \\ 0 & 0 & -1 \end{pmatrix}$
\hat{T}_{-1}	$2^{-1/2}\hat{I}_-$	$\begin{pmatrix} 0 & 0 & 0 \\ 1 & 0 & 0 \\ 0 & 1 & 0 \end{pmatrix}$
\hat{T}_{22}	$1/2\hat{I}_+^2$	$\begin{pmatrix} 0 & 0 & 1 \\ 0 & 0 & 0 \\ 0 & 0 & 0 \end{pmatrix}$
\hat{T}_{21}	$-1/2(\hat{I}_z\hat{I}_+ + \hat{I}_+\hat{I}_z)$	$2^{-1/2}\begin{pmatrix} 0 & -1 & 0 \\ 0 & 0 & 1 \\ 0 & 0 & 0 \end{pmatrix}$
\hat{T}_{20}	$6^{-1/2}(3\hat{I}_z^2 - \hat{I}^2)$	$6^{-1/2}\begin{pmatrix} 1 & 0 & 0 \\ 0 & -2 & 0 \\ 0 & 0 & 1 \end{pmatrix}$
\hat{T}_{2-1}	$1/2(\hat{I}_z\hat{I}_- + \hat{I}_-\hat{I}_z)$	$2^{-1/2}\begin{pmatrix} 0 & 0 & 0 \\ 1 & 0 & 0 \\ 0 & -1 & 0 \end{pmatrix}$
\hat{T}_{2-2}	$1/2\hat{I}_-^2$	$\begin{pmatrix} 0 & 0 & 0 \\ 0 & 0 & 0 \\ 1 & 0 & 0 \end{pmatrix}$

^a Brink and Satchler.¹⁹ ^b $|I, m\rangle$ basis.

The final form of the echo is in terms of the eigenvalues and eigenvectors of the stochastic Liouville operator, quantities which are regularly computed when calculating CW spectra.

Section II reviews the formalism and extends it to the calculation of quadrupole echoes. A recently published study¹⁵ of Hahn echoes (the $90^\circ-\tau-180^\circ-t$ sequence applied to ESR g-tensor [or NMR chemical shift tensor] and ESR hyperfine tensor Hamiltonians) should be consulted for further details and discussion. Section III describes the experimental parameters and sections IV and V present results and discussion.

II. Theory

Molecules whose rotational degrees of freedom are treated classically as a stationary Markov process and whose spin dynamics are treated quantum mechanically can be characterized by a density matrix $\hat{\rho}(\Omega, t)$ satisfying the stochastic Liouville equation of motion^{16,17}

$$\partial\hat{\rho}(\Omega, t)/\partial t = -i[\hat{H}(\Omega), \hat{\rho}(\Omega, t)] - \Gamma_\Omega[\hat{\rho}(\Omega, t) - \hat{\rho}_0(\Omega)] \quad (1)$$

where the Hamiltonian $\hat{H}(\Omega)$ depends on the orientation of the molecule specified by its Euler angles, $\Omega \equiv \alpha, \beta, \gamma$. Γ_Ω is the operator for the motional process, e.g., a diffusion operator, and $\hat{\rho}_0(\Omega)$ is the equilibrium density matrix.

The Hamiltonian is divided into three parts

(15) L. J. Schwartz, A. E. Stillman, and J. H. Freed, *J. Chem. Phys.*, **77**, 5410 (1982). Note that the approximation given in this reference to its eq 13 holds only for $n = 1$ and that the first term on the right-hand side of its eq 17c should not have a minus sign.

(16) (a) J. H. Freed, *J. Phys. Chem.*, **78**, 1115 (1974); (b) J. H. Freed in "Time Domain Electron Spin Resonance", L. Kevan and R. N. Schwartz, Eds., Wiley-Interscience, New York, 1979, Chapter 2.

(17) J. H. Freed in "Spin Labelling Theory and Applications", L. J. Berliner, Ed., Academic Press, New York, 1976, Chapter 3.

$$\hat{H}(\Omega) = \hat{H}_0 + \hat{H}_1(\Omega) + \hat{\varepsilon}(t) \quad (2)$$

For the deuterium nucleus in a high magnetic field, \hat{H}_0 is the nuclear Zeeman term (the chemical shift is taken to be isotropic), while $\hat{H}_1(\Omega)$ represents the quadrupole interaction. $\hat{H}_1(\Omega)$ is written in the laboratory frame (neglecting nonsecular terms) as¹⁸

$$\hat{H}_1(\Omega) = (e^2qQ/8)[(3 \cos^2 \beta - 1) + \eta \sin^2 \beta \cos 2\alpha][3\hat{I}_z^2 - \hat{I}^2] \quad (3)$$

$$= (e^2qQ/4)[6^{1/2}D_{00}^2(\Omega) + \eta(D_{20}^2(\Omega) + D_{-20}^2(\Omega))]\hat{T}_{20} \quad (4)$$

where D_{KM}^L are the Wigner rotation matrix elements and the \hat{T}_{lm} form the irreducible spherical tensor angular momentum operator basis set.¹⁹ The nine \hat{T}_{lm} for the spin $I = 1$ case are listed in Table I.

In the presence of a rotating field, the Hamiltonian includes the radiation term

$$\hat{\varepsilon}(t) = \frac{1}{2}\gamma_n B_1 [\hat{I}_+ \exp(-i\omega t) + \hat{I}_- \exp(i\omega t)] \quad (5)$$

where B_1 is the magnitude of the field.

The Markov operator Γ_Ω obeys

$$\partial P(\Omega, t) / \partial t = -\Gamma_\Omega P(\Omega, t) \quad (6)$$

where $P(\Omega, t)$ is the conditional probability density that a molecule is oriented with Euler angles between Ω and $\Omega + d\Omega$ at time t . The equilibrium probability distribution $P_0(\Omega)$ obeys $\Gamma_\Omega P_0(\Omega) = 0$, and the equilibrium density matrix $\rho_0(\Omega)$ in the high-temperature, high-field limit is

$$\hat{\rho}_0(\Omega) \simeq N^{-1}(1 - \hbar \hat{H}_0 / kT) \quad (7)$$

where N is the total number of spin eigenstates.^{16,17}

Because of the explicit time dependence of $\hat{\varepsilon}(t)$, it is convenient to rewrite eq 1 in terms of $\hat{\rho}_{\text{rf}}(\Omega, t)$, the density matrix in the frame rotating at the resonance frequency, ω . Then, to solve the rewritten eq 1, we assume that the radiation field is intense and short enough so that the sole effect of a pulse at frequency ω is a rotation of $\hat{\rho}_{\text{rf}}(\Omega, t)$ by some angle. That is, we assume that the $\hat{\varepsilon}(t)$ term dominates the spin Hamiltonian in the rotating frame and that, more generally, it dominates the stochastic Liouville operator during the infinitesimal pulse.

In the absence of radiation, eq 1 becomes

$$\partial \hat{\rho}_{\text{rf}}(\Omega, t) / \partial t = -A_{\text{rf}} \hat{\rho}_{\text{rf}}(\Omega, t) \quad (8)$$

where

$$A_{\text{rf}} \equiv -i[(\hat{H}_0 - \omega \hat{I}_z)^\times + \hat{H}_1(\Omega)^\times] - \Gamma_\Omega \quad (9)$$

the rotating frame stochastic Liouville operator; the superoperator notation \hat{H}^\times implies commutation of \hat{H} with what follows, i.e., $\hat{H}^\times \hat{U} \equiv [\hat{H}, \hat{U}]$. The solution to eq 8 is

$$\hat{\rho}_{\text{rf}}(\Omega, t + \tau) = \exp(-A_{\text{rf}} \tau) \hat{\rho}_{\text{rf}}(\Omega, t) \quad (10)$$

In the presence of the idealized pulse

$$A_{\text{rf}}^{\text{pulse}} = -i[(\hat{H}_0 - \omega \hat{I}_z)^\times + \hat{H}_1(\Omega)^\times + \hat{\varepsilon}(t)_{\text{rf}}^\times] - \Gamma_\Omega \quad (11)$$

$$\simeq -i\hat{\varepsilon}_{\text{rf}}^\times(t) \quad (12)$$

where $\hat{\varepsilon}_{\text{rf}}(t) = \gamma_n B_1 \hat{I}_x / \hbar$. Equation 1 becomes

$$\partial \hat{\rho}_{\text{rf}}(\Omega, t) / \partial t \simeq -i\hat{\varepsilon}_{\text{rf}}^\times \hat{\rho}_{\text{rf}}(\Omega, t) \quad (13)$$

with the solution

$$\hat{\rho}_{\text{rf}}(\Omega, t + \tau) = \exp(-i\hat{\varepsilon}_{\text{rf}}^\times \tau) \hat{\rho}_{\text{rf}}(\Omega, t) \quad (14)$$

Equation 14 is the usual transformation used to describe idealized pulses in analyses of spin echoes that do not

include motional modulation.

The effects of the rotations can be calculated by expanding the spin parts of the density matrix in the basis set which transforms according to the three-dimensional irreducible representation of the rotation group, i.e., in the basis of the spherical angular momentum operators, \hat{T}_{kq} , used earlier in the expression for $\hat{H}_1(\Omega)$ (see eq 4).²⁰ Under a rotation by angles (ϕ_1, ϕ_2, ϕ_3) , \hat{T}_{kq} transforms as

$$\hat{T}'_{kq} = \sum_p \hat{T}_{kp} D_{pq}^k(\phi_1, \phi_2, \phi_3) \quad (15)$$

The orientational degrees of freedom are incorporated into the density matrix by further expanding it in the complete orthonormal set of eigenfunctions of the diffusion operator, Γ_Ω . These are usually the generalized spherical harmonics (or Wigner rotation matrices), the $D_{KM}^L(\Omega)$. We therefore write

$$\hat{\rho}_{\text{rf}}(\Omega, t) = \sum_{LKM} C_{LKM,lm}(t) D_{KM}^L(\Omega) \hat{T}_{lm} \quad (16)$$

The NMR signal $S(t)$ can be expressed as

$$S(t) = \int P_0(\Omega) S(\Omega, t) d\Omega \quad (17)$$

$$\propto \text{tr} [\hat{\rho}(\Omega, t) \hat{T}_{11}] \quad (18)$$

where the superbar implies averaging over the equilibrium distribution in Ω . Under isotropic conditions where $P_0(\Omega)$ is a constant, it can be shown that

$$S(t) \propto C_{000,1-1}(t) \quad (19)$$

A similar expression can be written for anisotropic media.¹⁷

The effect of the 90°_y - τ - 90°_x - t quadrupole echo pulse sequence on the density matrix is calculated as follows. At $t = 0$

$$\hat{\rho}(\Omega, 0) \equiv \hat{\rho}_0(\Omega) \propto 1 - \hbar \hat{H}_0 / kT \quad (20)$$

$$\equiv 3^{1/2} \hat{T}_{00} - \epsilon \hat{T}_{10} \quad (21)$$

The identity, $3^{1/2} \hat{T}_{00}$, corresponds to the infinite temperature limit and is invariant to the rotations caused by the pulses. We can therefore neglect it and write

$$\hat{\rho}(\Omega, 0) = -\epsilon \hat{T}_{10} \quad (22)$$

i.e., initially $\hat{\rho}$ is independent of Ω .

According to eq 15, a 90°_y pulse transforms $\hat{\rho}(\Omega, 0)$ to

$$\hat{\rho}_{\text{rf}}(\Omega, 0^+) = \hat{\rho}(\Omega, 0^+) = (2^{-1/2})\epsilon(\hat{T}_{11} - \hat{T}_{1-1}) \quad (23)$$

During the evolution time τ , the stochastic Liouville operator introduces Ω dependence as well as two new spin components, proportional to \hat{T}_{21} and \hat{T}_{2-1} , into $\hat{\rho}(\Omega, t)$. The appearance of \hat{T}_{21} and \hat{T}_{2-1} is due to $\hat{H}_1(\Omega)$ acting on \hat{T}_{11} and \hat{T}_{1-1} ,²¹ while the time dependence of Ω arises from the Γ_Ω operator which is independent of spin. The $\hat{T}_{2\pm 2}$ components are not excited by $\hat{H}_1(\Omega)$ because $|\hat{H}_1(\Omega)| \ll |\hat{H}_0|$.²² The case for a finite T_1 , wherein the \hat{T}_{10} component can reappear, is presented in Appendix A.

$\hat{H}_1(\Omega)$ causes the $\hat{T}_{1\pm 1}$ components to evolve under coupled equations with the $\hat{T}_{2\pm 1}$ components. However, the linear combinations

$$\hat{T}_{1-1} \pm 2^{1/2} \hat{T}_{2-1} \quad (24)$$

$$\hat{T}_{11} \pm 2^{1/2} \hat{T}_{21} \quad (25)$$

(20) The expansion of the spin part of the density matrix in the \hat{T}_{lm} basis set is analogous to its expansion in the four Pauli spin operators in the $I = 1/2$ case.

(21) H. W. Spiess, *J. Chem. Phys.*, **72**, 6755 (1980).

(18) A. Abragam, "The Principles of Nuclear Magnetism", Clarendon Press, Oxford, 1961.

(19) D. M. Brink and G. R. Satchler, "Angular Momentum", 2nd ed., Clarendon Press, Oxford, 1971.

(22) (a) J. H. Freed, G. V. Bruno, and C. Polnaszek, *J. Chem. Phys.*, **55**, 5270 (1971); (b) E. Meirovitch and J. H. Freed, *Chem. Phys. Lett.*, **64**, 311 (1979).

are found to evolve independently. The pairs of linear combinations in expressions 24 and 25 each represent the two allowed single-quantum transitions of the quadrupole system (see Table I), but only the pair in expression 24 is important. The pair in expression 25 is the counterrotating pair and can be omitted from the calculation. In addition, because the two allowed transitions differ only in the sign of the quadrupole coupling constant, only one of the linear combinations in expression 24 needs to be followed through the evolution time with the stochastic Liouville operator as in eq 10; the other combination will yield the complex conjugate eigenvalues and eigenvectors in the solution of the stochastic Liouville equation.¹⁵

After the evolution time τ , the overall result is that

$$\hat{\rho}_{\text{rf}}(\Omega, \tau) = \exp(-A_{\text{rf}}\tau)\hat{\rho}_{\text{rf}}(\Omega, 0^+) \quad (26)$$

The effect of the second (i.e., 90°_x) pulse is calculated by returning to the \hat{T}_{lm} basis set and applying eq 15 to the \hat{T}_{1-1} and \hat{T}_{2-1} components of $\hat{\rho}_{\text{rf}}(\Omega, \tau)$. $\hat{\rho}_{\text{rf}}(\Omega, t)$ is Hermitian; also, due to the symmetry of the Hamiltonian with respect to the two allowed transitions, $\langle 0|\hat{\rho}|1\rangle = \langle 0|\hat{\rho}|1\rangle - 1$ and $\langle 1|\hat{\rho}|0\rangle = \langle -1|\hat{\rho}|0\rangle$. These restrictions lead to

$$\hat{\rho}_{\text{rf}}(\Omega, \tau^+) = \hat{\rho}_{\text{rf}}(\Omega, \tau)^* \quad (27)$$

The final evolution period is then treated analogously to the first, with the overall result that $\hat{\rho}_{\text{rf}}(\Omega, \tau^+)$ is transformed into

$$\hat{\rho}_{\text{rf}}(\Omega, \tau+t) = \exp(-A_{\text{rf}}t) \exp(-A_{\text{rf}}^*\tau)\hat{\rho}_{\text{rf}}^*(\Omega, 0^+) \quad (28)$$

The signal intensity at the end of the pulse sequence ultimately depends only on the coefficient of the \hat{T}_{1-1} spin component, $\sum_{LKM} C_{LKM,1-1}(\tau+t) D_{KM}^L(\Omega)$. The $C_{LKM,1-1}(\tau+t)$ can be viewed as the components of a vector $\mathbf{C}(\tau+t)$ which obeys

$$\mathbf{C}(\tau+t) = \exp(-Bt) \exp(-B^*\tau)\mathbf{U} \quad (29)$$

where the matrix B is obtained from A_{rf} .²³ The dimension of $\mathbf{C}(t)$ is $L_{\text{max}} \times K_{\text{max}}$ ($M=0$) and $\mathbf{C}(0^+) \equiv \mathbf{U}$ is the unit vector, nonzero only for the $L=K=0$ basis element.

The observed NMR signal (along the x axis) is then

$$S(\tau+t) \propto \text{Re} [\mathbf{U}^{\text{tr}} \exp(-Bt) \exp(-B^*\tau)\mathbf{U}] \quad (30)$$

In terms of the eigenvector O and eigenvalue Λ matrices of B (with $O^{-1}BO = \Lambda$ and $O^{-1} = O^{\text{tr}}$)

$$S(\tau+t) \propto \text{Re} [\mathbf{U}^{\text{tr}}O \exp(-\Lambda t)O^{\text{tr}}O^* \exp(-\Lambda^*\tau)O^{*\text{tr}}\mathbf{U}^*] \quad (31)$$

or

$$S(\tau+t) \propto \text{Re} \sum_{\substack{ijk \\ lm}} U_k O_{kl} O_{il} O_{ij}^* O_{mj}^* U_m^* \exp[-(\Lambda_i t + \Lambda_j^* \tau)] \quad (32)$$

$$\equiv \text{Re} \sum_{ij} a_{ij} \exp[-(\Lambda_i t + \Lambda_j^* \tau)] \quad (33)$$

Equation 32 can also be derived by taking advantage of

(23) A_{rf} is first multiplied by $D_{KM}^L(\Omega)$ and integrated over all Ω to give the angular average.¹⁷ Next, A_{rf} is multiplied by \hat{T}_{lm}^* and the trace is taken. This step generates triple products $\text{tr}(\hat{T}_{lm}^* \hat{T}_{20} \hat{T}_{lm})$ where \hat{T}_{20} comes from $\hat{H}_1(\Omega)$. These products are evaluated by applying the product rule for pairs of \hat{T}_{lm} 's and then noting the orthogonality of the \hat{T}_{lm} 's under the trace operation. [See L. C. Biedenharn and J. D. Louck in the "Encyclopedia of Mathematics and Its Applications", G.-C. Rota, Ed., Addison-Wesley, London, 1981, p 462.]

(24) Because $I=1$ quadrupole spectra can be regarded as a superposition of spectra due to the two allowed single-quantum transitions^{22b} the formalism of ref 15 can be used for each transition separately, which are then added together. The calculations are simplified by the fact that the eigenvalues and eigenvectors for the two transitions are complex conjugates of each other.

the formal equivalence between the spin $I=1$ quadrupole Hamiltonian and that incorporating the dipolar interaction of two spin $I=1/2$ nuclei.²⁴

In the presence of imperfect (i.e., not $\pi/2$) pulses, the final expression for the coefficient of the \hat{T}_{1-1} spin basis component can include effects mixed in not only by the \hat{T}_{2-1} component but by the \hat{T}_{10} component as well. (\hat{T}_{20} and $\hat{T}_{2\pm 2}$ components can also appear, but they will not affect the final form of the observable \hat{T}_{1-1} component; see ref 21.) However, it is still a completely straightforward procedure to write down the resulting expression for \hat{T}_{1-1} with the aid of eq 15. A more involved case is when $|\gamma_n B_1| \leq |\hat{H}_1(\Omega)|$, so that the effect of the pulses cannot be regarded as simple rotations, and all of the density matrix elements can be mixed in by the pulses. Equation 12-14 would no longer be rigorous, but eq 11 can be rigorously solved by the present approach to yield results analogous to those obtained by Vega and Pines.²⁵ Ultimately, the difficult problem is the experimental one of knowing the exact character of the pulses being modeled. At present, nonideal pulses must be regarded as a possible source of error in comparing experiment and theory.

Finally, inhomogeneous broadening multiplies $S(\tau+t)$ by the Fourier transform of the frequency broadening distribution function (see Appendix B), so for Lorentzian broadening

$$S(\tau+t) \propto \exp[-\Gamma(t-\tau)] \text{Re} \sum_{ij} a_{ij} \exp[-(\Lambda_i t + \Lambda_j^* \tau)] \quad (34)$$

while for Gaussian broadening

$$S(\tau+t) \propto \exp[-(t-\tau)^2 \Gamma^2 / 4 \ln 2] \text{Re} \sum_{ij} a_{ij} \exp[-(\Lambda_i t + \Lambda_j^* \tau)] \quad (35)$$

where Γ is the half-width at half-height of the distribution function.

III. Experimental Section

Trimethylsulphoxonium- d_9 iodide was prepared from dimethyl- d_6 sulfoxide and methyl- d_3 iodide.²⁶ These deuterated starting materials, as well as the hexamethylbenzene- d_{18} , were purchased from Merck Sharp and Dohme, Montreal.

^2H NMR spectra were obtained at a radiofrequency of 27.6 MHz on a Bruker CXP-180 NMR spectrometer. Half-echoes, obtained by using the phase-alternated quadrupole echo sequence,^{6b} were digitized at a sweep width setting of 250 kHz. The 90° pulse length was 2.6 μs and the spacing, τ , between the two phase-shifted pulses was 30 μs . The pulse repetition rate was slow enough to avoid problems with T_1 relaxation (see also Appendix A). Spectra were carefully checked with full quadrature detection²⁷ to ensure that they were symmetrical about their center before they were recorded. The 1K point half-echoes were zero filled to give 4K data points before Fourier transformation.

IV. Results and Discussion

Hexamethylbenzene- d_{18} (HMB- d_{18}). Experimental ^2H quadrupole echo spectra of a polycrystalline powder of $\text{C}_6(\text{CD}_3)_6$ in the temperature range 130-240 K are presented in Figure 2. The highest and lowest temperature spectra are quite close to being characteristic of axially symmetric ^2H NMR powder spectra. Deviations from axial

(25) S. Vega and A. Pines, *J. Chem. Phys.*, **66**, 5624 (1977).

(26) J. A. Ripmeester, *Can. J. Chem.*, **59**, 1671 (1981).

(27) R. G. Griffin, "Methods in Enzymology", Vol. 72, Academic Press, New York, 1981.

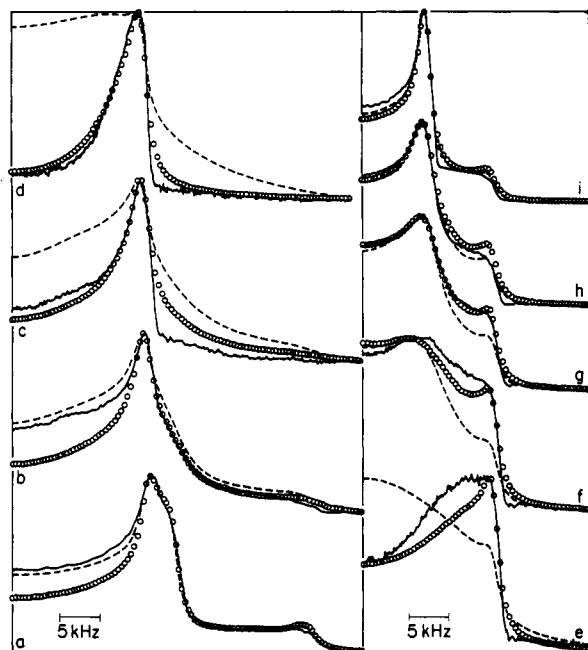


Figure 2. Experimental and simulated hexamethylbenzene- d_{18} NMR spectra: (solid lines) experimental results, (open circles) simulations from quadrupole echo calculations with $\tau = 30 \mu\text{s}$, (dashed lines) simulation from calculated free induction decays. The simulations⁴² incorporate a 6-fold jump model. The temperatures and jump rates, τ_J^{-1} , are as follows: (a) 130 K, $\tau_J^{-1} = 0$; (b) 150 K, $\tau_J^{-1} = 3.0 \times 10^9 \text{ s}^{-1}$; (c) 160 K, $\tau_J^{-1} = 6.0 \times 10^9 \text{ s}^{-1}$; (d) 170 K, $\tau_J^{-1} = 1.8 \times 10^4 \text{ s}^{-1}$; (e) 180 K, $\tau_J^{-1} = 5.4 \times 10^4 \text{ s}^{-1}$; (f) 190 K, $\tau_J^{-1} = 1.5 \times 10^5 \text{ s}^{-1}$; (g) 200 K, $\tau_J^{-1} = 2.7 \times 10^5 \text{ s}^{-1}$; (h) 210 K, $\tau_J^{-1} = 4.5 \times 10^5 \text{ s}^{-1}$; (i) 240 K, $\tau_J^{-1} = 1.8 \times 10^6 \text{ s}^{-1}$.

symmetry show up as a small shoulder on the high-frequency side of the dominant peak and in the fact that the frequency difference between the center of the spectrum and the dominant peak is not exactly one-half of that between the center and the high-frequency shoulder (the dominant peak is due to molecules whose quadrupole tensor is oriented approximately perpendicularly to the external field, while the high-frequency shoulder results from quadrupole tensors oriented approximately parallel to the external field).

The quadrupole coupling constant, e^2qQ , can be estimated directly from a true rigid limit spectrum as the frequency difference between the dominant peaks, which is equal to $3e^2qQ/4$. Assuming that the 130 K spectrum is undistorted, its calculated coupling constant is $\approx 51 \text{ kHz}$. Coupling constants of aliphatic deuterons generally range between 160 and 190 kHz;²⁸ in particular, that of $\text{CD}_3\text{C}_6\text{H}_5$ is 165 kHz.²⁹ In contrast, the measured coupling constant of the methyl deuterons in toluene- d_8 at 77 K is $52.0 \pm 1.4 \text{ kHz}$,³⁰ consistent with our measured result. The smaller value corresponds to a partially averaged quadrupole tensor arising from fast internal methyl rotation (see Figure 1). Indeed, under rapid reorientation about an axis (i.e., the aliphatic C-C bond in HMB- d_{18}) tilted by θ° relative to the z principal axis of the quadrupole tensor (taken to be along the HMB- d_{18} C-D bond), an axially symmetric rigid limit powder pattern changes into a "reduced" axially symmetric spectrum corresponding to an effective coupling constant $1/2(e^2qQ)(3 \cos^2 \theta - 1)$. For tetrahedral coordination, $\theta \approx 70^\circ$, so that, assuming that e^2qQ actually equals

TABLE II: Experimental T_2 Values for Hexamethylbenzene- d_{18} ^a

temp, K	$T_2, \mu\text{s}$	temp, K	$T_2, \mu\text{s}$
143	370	183	150
153	120	193	360
173	60	223	800

^a Obtained by Vega.³³

$\approx 165 \text{ kHz}$ for HMB- d_{18} , we would predict a measured, effective quadrupole coupling constant of 54 kHz in the axially symmetric case.³¹

We will therefore assume that the internal methyl rotation is in its motional narrowing limit at 130 K (i.e., the motional rate is rapid on the ^2H NMR time scale) and that the changes in the spectra between 130 and 240 K arise from a different dynamic process. Note that the 240 K spectrum is very similar to the 130 K spectrum except that its effective coupling constant has been reduced by one-half. By the same logic as just employed, such a reduction implies a second averaging about an axis tilted by 90° with respect to the principal axis of the already averaged quadrupole tensor. This second motional averaging process is therefore about an axis perpendicular to the benzene ring corresponding to interchange of the entire methyl groups, and it has approximately reached its motional narrowing limit at 240 K. The remaining nonaxial symmetry of the high-temperature spectrum might be related to distortion of the benzene ring from a perfect hexagon.¹³

A previous study, using line-shape analysis of ^{13}C spectra of HMB, has shown that the reorientation of HMB takes place via 6-fold discrete jumps about the perpendicular (hexad) axis.³ Quadrupole echo spectra simulated by using the 6-fold discrete jump model are shown in Figure 2 along with the jump rates, τ_J^{-1} (note that the rotational correlation times are $\tau_R = \tau_J/3$).³² Also shown in Figure 2 are Fourier-transformed free induction decays. While the spectra from the free induction decays fit the experimental spectra for the two temperature extremes, it is clear that a full echo treatment is needed to reproduce the spectra at the intermediate temperatures (160–190 K). Echo "distortions" are expected whenever the time τ between pulses is comparable to the phase memory times T_M of the individual components in the powder spectrum, provided that these components relax with different T_M 's.^{7,8} (These components correspond to different orientations of the quadrupole tensor with respect to the applied external field.) Table II lists overall experimental T_2 values for HMB- d_{18} obtained by Vega.³³ The parallel between increasing "distortion" present in the experimental spectra (i.e., increasing difference between the spectra calculated from simulated fid's vs. from simulated echoes) and T_2 approaching τ ($\tau = 30 \mu\text{s}$) is obvious.

Spectra were also simulated for two other highly anisotropic diffusion models: Brownian diffusion, and random jumps with the average jump angle $\approx 57^\circ$ (i.e., $R\tau_J = 1$, with $R \equiv$ rotational diffusion coefficient and $\tau_J \equiv$ average time between jumps). In all cases, motion was about the axis perpendicular to the benzene ring. These two models give spectra which are indistinguishable from those incorporating the 6-fold discrete jump model shown

(31) It is possible that the appearance of an apparent asymmetry parameter may be due to unresolved dipolar couplings [see N. Boden, L. D. Clark, S. M. Hanlon, and M. Mortimer, *Faraday Symp. Chem. Soc.*, No. 13, 109 (1978)], although one would expect to observe it for both HMB- d_{18} and TMSI- d_9 .

(32) A. Baram, Z. Luz, and S. Alexander, *J. Chem. Phys.*, 64, 4321 (1976).

(33) A. Vega, Du Pont Co., Wilmington, DE 19898, private communication.

(28) H. H. Matsch, H. Saito, I. C. P. Smith, *Prog. Nucl. Magn. Reson. Spectrosc.*, 11, 211 (1977).

(29) J. C. Rowell, W. D. Phillips, L. R. Melby, and M. Panar, *J. Chem. Phys.*, 43, 3442 (1965).

(30) R. G. Barnes in "Advances in Nuclear Quadrupole Resonance", Vol. 1, J. A. S. Smith, Ed., Heyden, London, 1972, Chapter 26.

in Figure 2, but they give rotational correlation times larger by a factor of ≈ 10 . Such a result was also found in recent ESR studies³⁴ of slow planar motions on surfaces, where large differences in τ_R were predicted by different motional models.

One might be tempted to try to choose between 6-fold jumps and Brownian and random jump diffusion by seeing which model(s) predict τ_R satisfying $|\hat{H}_1(\Omega)|\tau_R \approx 1$ at the temperature for which T_2 is a minimum. This relationship was found to be a reasonable criterion for isotropic motions in our previous study¹⁵ of slow motions and Hahn echoes. It is not simple, however, to calculate $|\hat{H}_1(\Omega)|$ in the presence of highly anisotropic motion, since such motion can average only a portion of the total width of the spectrum due to each of the single transitions, and, for each molecule, that portion will depend on the orientation of the principal axis of the molecule with respect to the applied field.

Another way to try to discriminate between the motional models is by calculating echo envelopes ($90^\circ_y - \tau - 90^\circ_x - \tau$ sequences run as a function of τ) for the parameters used to simulate the spectra in Figure 2 and comparing the resulting phase memory times, T_M , with the T_2 data presented in Table II. Previous theoretical work¹⁵ has shown that, at least for isotropic motion, the relationship between T_M and τ_R is model dependent. We have calculated echo envelopes for HMB- d_{18} using the 6-fold jump and Brownian models. The 6-fold jump envelopes are highly nonexponential and are thus difficult to characterize with a single decay constant; the Brownian envelopes deviate less so from exponential behavior. Fitting the envelopes roughly, however, the two models predict the same T_M curve as a function of temperature. Unfortunately, the model dependence of T_M on τ_R appears to be compensated by the different τ_R 's predicted by the two models in the line-shape study. Therefore, we are left to simply note that, in the present study, the 6-fold jump model is the one consistent with the HMB ^{13}C study as mentioned above,³ and so we take it to be the correct model.³⁵

The fact that there is no difference in the simulated HMB- d_{18} line shapes with respect to Brownian, random jump, and 6-fold jump motions is in contrast to that found in the ^{13}C NMR study of the ring carbons of HMB: Spectra from that study contain features which clearly favor a 6-fold jump process over Brownian diffusion. (This previous study³ was not performed with echoes; however, we also find in the present study no differences, for the three motional models, in spectra calculated from free induction decays.)

The lack of sensitivity to motional details of the ^2H HMB- d_{18} spectra as compared to the ^{13}C HMB spectra can be rationalized by comparing the latter with spectra calculated for a single transition of the quadrupole system,^{24,30,32} as shown schematically in Figure 3. Motion of the HMB- d_{18} molecule about its C_6 axis (the molecular z axis) averages together the magnetic tensor components which lie along the x and y axes. The ^{13}C magnetic

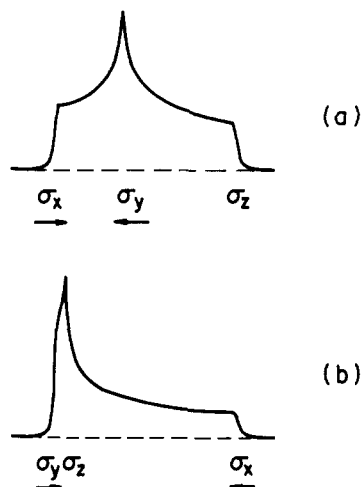


Figure 3. Schematic powder spectra of hexamethylbenzene- d_{18} showing the principal components of the magnetic tensors: (a) ^{13}C NMR spectrum, σ is the chemical shift tensor; (b) ^2H NMR spectral component due to only one of the two allowed spin transitions, σ is the quadrupole tensor. The arrows show the directions in which the spectra change as the molecule executes jumps about its molecular z axis.

chemical shift tensor is such that, as its components along the molecular x and y axes are more and more effectively averaged together by the molecular motion, the resulting jump structure in the spectrum (located between that due to the components along the x and y axes) can be and is clearly exposed. The ^2H quadrupole tensor, however, is such that jump structure will be "hidden" by the portion of the spectrum which is invariant to the motion of the molecule about its molecular z axis. Therefore, although the deuterium HMB- d_{18} spectra are sensitive enough to show the two (or three) different environments felt by the three methyl deuterium atoms (resulting in the nonaxially symmetric spectra at 130 and 240 K), they are not sensitive enough to distinguish different types of motion.

We now compare in detail our calculated HMB- d_{18} 6-fold rotational correlation times with previously reported data. Allen and Cowking¹² have fitted HMB correlation times in the temperature region 150–200 K to an Arrhenius curve

$$\tau_R = \tau_0 \exp(E_A/RT) \quad (36)$$

with $E_A = 6.7 \pm 0.1$ kcal/mol and $\tau_0 \approx 1.2 \times 10^{-14}$ s. (See also ref 13.) Also, as mentioned above, Wemmer³ has fitted ^{13}C line shapes of HMB at some of the temperatures included in this study using the 6-fold jump model. A T_1 study of HMB- d_{18} by Tang et al.¹⁰ in the temperature range 190–343 K reports $E_A = 7.8 \pm 0.1$ kcal/mol and $\tau_0 \approx 1.8 \times 10^{-15}$ s. Correlation times from the present study give $E_A = 5.30 \pm 0.2$ kcal/mol and $\tau_0 \approx 2 \times 10^{-12}$ s for HMB- d_{18} .

From separate comparisons of the two studies of HMB, and of the two studies of HMB- d_{18} , it appears that the precision of the results exceeds their accuracy. Each pair of studies (including a HMB study by Rothwell and Waugh¹⁴) does show good agreement, however, at temperatures of ≈ 170 – 180 K (temperatures at which T_2 is a minimum; see Table II). The correlation times at 175 K are 3.2×10^{-6} (ref 12) and 4.4×10^{-6} (ref 14) s for HMB, and 1.2×10^{-5} (ref 10) and 0.98×10^{-5} (present study) s for HMB- d_{18} , implying an almost 3-fold increase in τ_R with deuteration. At other temperatures, there is less agreement within each pair of studies, but the τ_R 's for the deuterated molecule are found to be consistently larger than for the undeuterated one.

(34) (a) M. Shiotani, G. Moro, and J. H. Freed, *J. Chem. Phys.*, **74**, 3757 (1981); (b) M. Shiotani and J. H. Freed, *J. Phys. Chem.*, **85**, 3873 (1981).

(35) One might also try to compare the τ_R 's predicted by the 6-fold jump model and the Brownian and random jump models with results previously obtained by T_1 ¹² and T_2 ¹⁴ (in the presence of an rf decoupling field) measurements, since these analyses were based on fast-motional theory and should therefore be model independent. However, as we note above (and in Appendix A), and as shown by Tang et al.,¹⁰ the T_1 's and T_2 's for anisotropic motions explicitly depend upon the angle of tilt between the molecular principal axis and the external field. Nevertheless, these previous results are found to be in agreement (within the isotope effect discussed later on) with the τ_R 's predicted by the 6-fold jump model spectra presented in Figure 2.

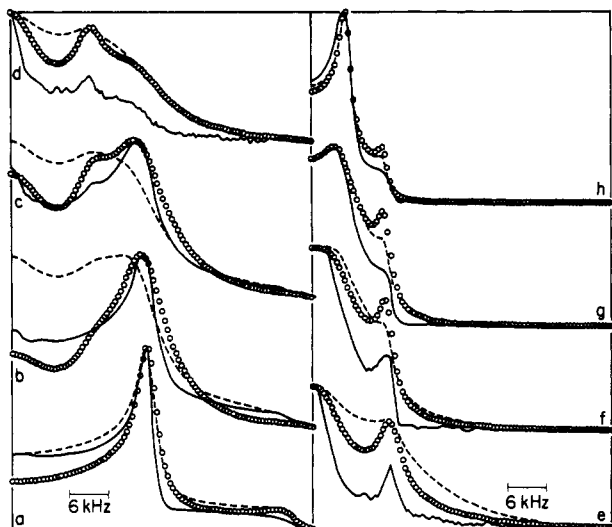


Figure 4. Experimental and simulated trimethylsulfoxonium- d_9 iodide NMR spectra: (solid lines) experimental results, (open circles) simulations from quadrupole echo calculations with $\tau = 30 \mu\text{s}$, (dashed lines) simulations from calculated free induction decays. The simulations⁴² incorporate a 3-fold jump axis tilted with respect to the C-S bond by 67.5° . The temperatures and jump rates, τ_J^{-1} are as follows: (a) 286 K, $\tau_J^{-1} = 0$; (b) 306 K, $\tau_J^{-1} = 8.4 \times 10^3 \text{ s}^{-1}$; (c) 316 K, $\tau_J^{-1} = 1.1 \times 10^4 \text{ s}^{-1}$; (d) 326 K, $\tau_J^{-1} = 1.4 \times 10^4 \text{ s}^{-1}$; (e) 336 K, $\tau_J^{-1} = 2.7 \times 10^4 \text{ s}^{-1}$; (f) 366 K, $\tau_J^{-1} = 9.0 \times 10^4 \text{ s}^{-1}$; (g) 376 K, $\tau_J^{-1} = 1.5 \times 10^5 \text{ s}^{-1}$; (h) 396 K, $\tau_J^{-1} = 6.0 \times 10^5 \text{ s}^{-1}$.

Finally, as justification for omitting T_1 effects in the present paper, we note that experimental T_1 measurements on a single crystal of hexamethylbenzene- d_{18} ¹⁰ oriented with its C_6 axis parallel to the external field (so that the anisotropic T_1 is minimized) gave the minimum T_1 to be $\approx 6 \text{ ms}$ at $\approx 267 \text{ K}$. The time scale for the experiments described in this paper is microseconds, and T_1 effects were therefore not included.

Trimethylsulfoxonium- d_9 Iodide (TMSI- d_9). Experimental ^2H quadrupole echo spectra of a polycrystalline powder of $(\text{CD}_3)_3\text{SO}^+\text{I}^-$ in the temperature range 286–396 K are presented in Figure 4. The lowest and highest temperature spectra are axially symmetric, with measured coupling constants of 57 and 14 kHz, respectively. The magnitude of the low-temperature coupling constant can be rationalized in terms of fast-motional tetrahedral methyl averaging, as was done earlier for HMB- d_{18} . The nearly 4-fold reduction in the magnitude of the coupling constant from 286 to 396 K implies that the tilt angle between the diffusive axis and the principal averaged quadrupole tensor axis (along the S-C bond) for the second process must be on the order of either 42° or 65° . (Because the spectra are symmetric, positive and negative values of $\frac{1}{2}(3 \cos^2 \theta - 1)$ are not distinguishable.) The tilt angle was therefore a variable in the simulations.

In contrast to the HMB- d_{18} spectra, the unusual features of the experimental spectra suggest a jump-type motional process rather than continuous diffusion.³² The simulated spectra in Figure 4 incorporate 3-fold jumps about an axis tilted 67.5° with respect to the S-C bond. Highly anisotropic Brownian and random jump diffusion about the same axis completely failed to reproduce the experimental spectral features.

The simulated spectra are very sensitive to the tilt angle. Spectra were calculated for $40^\circ \leq \theta \leq 50^\circ$ and $60^\circ \leq \theta \leq 70^\circ$, with best fits occurring for $\theta = 67.5^\circ$. To illustrate the high accuracy to which θ can be determined, Figure 5 shows line shapes calculated by using the jump rate which best fits the most "sensitive" spectrum, that of 336 K, for a range of tilt angles. In particular, note that, within

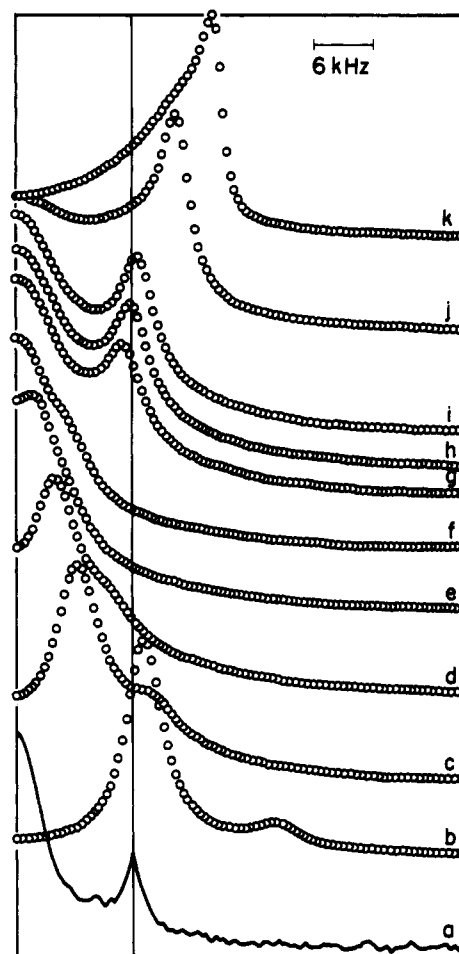


Figure 5. Simulated⁴² trimethylsulfoxonium- d_9 iodide line shapes as a function of θ , the tilt angle between the C_{3v} jump axis and the C-S bond: (a) experimental 336 K spectrum; for b-k τ_J^{-1} , the jump rate, is $3.0 \times 10^3 \text{ s}^{-1}$; (b) $\theta = 30^\circ$, (c) $\theta = 42^\circ$, (d) $\theta = 46^\circ$, (e) $\theta = 50^\circ$, (f) $\theta = 60^\circ$, (g) $\theta = 66.5^\circ$, (h) $\theta = 67.5^\circ$ (best fit to the experimental spectrum), (i) $\theta = 68.5^\circ$, (j) $\theta = 75^\circ$, (k) $\theta = 90^\circ$.

the resolution of the experimental spectrum, $\theta = 67.5^\circ$ is easily distinguishable from $\theta = 66.5^\circ$ and $\theta = 68.5^\circ$.

X-ray crystallographic studies³⁶ have been performed on $[(\text{CH}_3)_3\text{SO}]^+\text{ClO}_4^-$ and $[(\text{CH}_3)_3\text{SO}]^+\text{BF}_4^-$. Both studies report inequivalent O-S-C angles among the three methyl groups. For $[(\text{CH}_3)_3\text{SO}]^+\text{ClO}_4^-$, the two inequivalent angles are $67.9 \pm 0.5^\circ$ and $65.2 \pm 0.6^\circ$, while for $[(\text{CH}_3)_3\text{SO}]^+\text{BF}_4^-$, the three inequivalent angles are $67.4 \pm 0.7^\circ$, $67.9 \pm 0.7^\circ$, and $67.3 \pm 0.7^\circ$. Bond angle inequivalence does not show up in the TMSI- d_9 spectra in Figure 4, however.

The range of temperatures for TMSI- d_9 for which quadrupole echo calculations give results different from free induction decay calculations (306–316 K) is close to the approximate rigid limit temperature, 286 K. Even for the higher temperatures (326–366 K), the echo calculations give better resolution than do the more "smeared-out" fid results. Indeed, fits of the experimental spectra to calculated fid spectra erroneously predict the tilt angle θ to be $\approx 66.5^\circ$, rather than the 67.5° predicted by the echo fits.

The cause of the overall intensity difference between several of the calculated and experimental spectra is unknown. This type of experimental observation has been used as a hint of the effectiveness of an additional slow process.²⁷ The loss of experimental intensity might also be due to the finite pulse widths.³⁷

(36) (a) I. C. Zimmermann, M. Barlow, and J. D. McCullough, *Acta Crystallogr.*, 16, 676 (1963); (b) C. L. Coulter, P. K. Gantzel, and J. D. McCullough, *ibid.*, 16, 883 (1963).

A least-squares fit of τ_R to $1/T$ for the 3-fold jump model gives $E_A = 11.1 \pm 0.9$ kcal/mol and $\tau_0 \approx 6 \times 10^{-13}$ s for TMSI- d_9 . A previous study¹¹ of TMSI using second moment, T_1 , and $T_{1\rho}$ measurements reports $E_A \approx 11.2$ kcal/mol and $\tau_0 \approx 5 \times 10^{-13}$ s, in excellent agreement with our results. It is interesting that, in contrast to HMB and HMB- d_{18} , the rotational correlation times of TMSI do not appear to change upon its deuteration to TMSI- d_9 .

V. Summary

We have shown in this work how dynamic quadrupole echo simulations can aid in, and indeed are indispensable for, the proper interpretation of deuterium quadrupole echo spectra. Two polycrystalline materials, hexamethylbenzene- d_{18} and trimethylsulphoxonium- d_9 iodide, were studied with the aim of learning about internal motions in solids. Both materials were found to exhibit two approximately independent motional modes: methyl rotational averaging, and the interchange of entire methyl groups about a single axis. The HMB- d_{18} spectra do not distinguish between a 6-fold jump process, Brownian and random jump diffusion for this latter process all taken about the hexad axis. In contrast, the TMSI- d_9 spectra clearly favor 3-fold jumps and predict a tilt angle of the O-S bond relative to the S-C bond of $67.5 \pm 1.0^\circ$. Activation energies and inverse frequency factors for the two compounds were calculated to be 5.3 ± 0.2 kcal/mol and $\approx 2 \times 10^{-12}$ s for HMB- d_{18} and 11.1 ± 0.9 kcal/mol and $\approx 6 \times 10^{-13}$ s for TMSI- d_9 , respectively.

The effect of deuteration on the correlation times appears to be an increase for HMB- d_{18} ,¹⁰ with no change found for TMSI- d_9 .

Acknowledgment. We thank Dr. Alexander Vega³³ for permission to include his hexamethylbenzene- d_{18} T_2 data, given in Table II, and acknowledge a helpful conversation with Dr. T. K. Halstead on the use of the spherical tensor basis set for the expansion of $\hat{\rho}(\Omega, t)$. This research was supported by NSF Grant No. CHE8024124, NIH Grant No. GM25862, and the Charles H. Revson Foundation.

Appendix A

Inclusion of T_1 Effects in the Echo Calculation. The slow-motional stochastic Liouville equation expressions for the relaxation of the diagonal density matrix elements (i.e., the $m = -1, 0, 1$ diagonal density matrix elements written in the $|I, m\rangle$ basis; see Table I) for the spin $I = 1$ case are given in ref 38 and 39. Nonsecular terms of the Hamiltonian are explicitly included. In the limit $|\omega_0| \gg \tau_{LK}^{-1}$, $|e^2qQ|$ (where τ_{LK} ^{17,32} are the eigenvalues of the diffusion operator; L, K are indices from the $D_{KM}^L(\Omega)$ function), these expressions may be greatly simplified by the use of perturbation theory^{39,40} on the nonsecular terms.

By analogy to eq 16 in the text, we define

$$\hat{\chi}_{\text{rf}}(\Omega, t) = \sum_{LKM} C'_{LKM,lm}(t) D_{KM}^L(\Omega) \hat{T}_{lm} \quad (\text{A1})$$

where $\hat{\chi}_{\text{rf}}(\Omega, t) \equiv \hat{\rho}_{\text{rf}}(\Omega, t) - \hat{\rho}_0(\Omega)$. Note that the deviations of the diagonal density matrix elements from equilibrium are represented by the $l, m = 10, 00$, and 20 terms in the sum. These three terms obey uncoupled rate equations in the absence of pulses:

$$\dot{C}'_{LKM,10}(t) = -(\tau_{LK} + [W_I + 2W_x]\delta_{L0}\delta_{K0})C'_{LKM,10}(t) \quad (\text{A2})$$

$$\dot{C}'_{LKM,00}(t) = -\tau_{LK}^{-1}C'_{LKM,00}(t) \quad (\text{A3})$$

$$\dot{C}'_{LKM,20}(t) = -(\tau_{LK}^{-1} + 3W_I\delta_{L0}\delta_{K0})C'_{LKM,20}(t) \quad (\text{A4})$$

W_I and W_x refer respectively to the electric quadrupole and induced single-quantum ($\Delta m = \pm 1$) and double-quantum ($\Delta m = \pm 2$) relaxation transition rates, which are found to be identical with the results from fast-motional spin relaxation theory in the limit $\tau_{LK}\omega_0 \gg 1$ ³⁹ where $L = 2$.

For isotropic Brownian diffusion¹⁸

$$\tau_{LK}^{-1} = L(L+1)R \quad (\text{A5})$$

$$W_I = AJ(\omega_0) \quad (\text{A6})$$

$$W_x = 2AJ(\omega_0) \quad (\text{A7})$$

$$J(\omega) = 6R/\omega^2 \quad (\text{A8})$$

$$A = (3/40)(1 + \eta^2/3)(e^2qQ/h)^2 \quad (\text{A9})$$

where R is the rotational diffusion coefficient.

For anisotropic diffusion and/or internal rotation about the principal molecular axes,^{5,22b}

$$\tau_{LK}^{-1} = L(L+1)R_{\perp} + K^2(R_{\parallel} - R_{\perp}) + K^2R_i \quad (\text{A10})$$

$$\equiv [L(L+1) - K^2]R_{\perp} + K^2R'_{\parallel} \quad (\text{A11})$$

while for discrete jumps about an axis among equivalent sites³²

$$\tau_{LK}^{-1} = (2/\tau_J)(1 - \cos(\kappa\beta)) \quad (\text{A12})$$

where R'_{\parallel} and R_{\perp} are effective rotational diffusion coefficients for motions parallel and perpendicular to the molecular z axis, respectively, R_i is the diffusion coefficient for internal rotations parallel to the z axis, β is the discrete jump angle, and τ_J is the time between jumps. Then for $\eta = 0$ ^{40a}

$$W_I = A\{|f^{(0)}|^2 J_0(\omega_0) + 2|f^{(1)}|^2 J_1(\omega_0) + 2|f^{(2)}|^2 J_2(\omega_0)\} \quad (\text{A13})$$

$$W_x = 2A\{|f^{(0)}|^2 J_0(2\omega_0) + 2|f^{(1)}|^2 J_1(2\omega_0) + 2|f^{(2)}|^2 J_2(2\omega_0)\} \quad (\text{A14})$$

$$J_K(\omega) = (\omega^2 \tau_{2K})^{-1} \quad (\text{A15})$$

$$|f^{(0)}|^2 = \frac{1}{4}(1 - 3 \cos^2 \theta)^2 \quad (\text{A16})$$

$$|f^{(1)}|^2 = \frac{3}{2} \sin^2 \theta \cos^2 \theta \quad (\text{A17})$$

$$|f^{(2)}|^2 = \frac{3}{8} \sin^4 \theta \quad (\text{A18})$$

where θ is the angle between the quadrupolar z axis and the diffusion z axis. Note that in the limit $R_{\perp} \ll R'_{\parallel}$, the terms in R'_{\parallel} provide the dominant contribution.⁴¹

The solutions to eq A2-A4 are

$$C'_{LKM,10}(t) = a_{LKM,10} \exp[-(\tau_{LK}^{-1} + [W_I + 2W_x]\delta_{L0}\delta_{K0})t] \quad (\text{A19})$$

$$C'_{LKM,00}(t) = a_{LKM,00} \exp[-\tau_{LK}^{-1}t] \quad (\text{A20})$$

$$C'_{LKM,20}(t) = a_{LKM,20} \exp[-(\tau_{LK}^{-1} + 3W_I\delta_{L0}\delta_{K0})t] \quad (\text{A21})$$

(41) In the limit $R_{\perp} \rightarrow 0$ one can define an angular-dependent $T_1^{-1}(\theta)$, where θ is the angle between the molecular axis of internal rotation and the magnetic field.^{39,40a} For a polycrystalline sample, one would then average over θ . Our method implicitly performs this averaging.

(42) A small, overall isotropic Brownian diffusion coefficient is included in all the calculations to aid computational convergence. It does not essentially change the features of the spectra, but acts instead like inhomogeneous broadening. The total inhomogeneous broadening added onto the simulated spectra must therefore be estimated, and is ≈ 0.15 kHz for HMB- d_{18} and ≈ 0.85 kHz for TMSI- d_9 . The $\tau_J^{-1} = 0$ TMSI- d_9 spectrum has an additional 0.84 kHz broadening. No difference is seen between Lorentzian and Gaussian broadening.

(37) M. Bloom, J. H. Davis, and M. I. Valic, *Can. J. Phys.*, **58**, 1510 (1980).

(38) G. V. Bruno, Ph.D. Thesis, Cornell University, Ithaca, NY, 1973.

(39) J. H. Freed, G. V. Bruno, and C. F. Polnaszek, *J. Phys. Chem.*, **75**, 3385 (1971).

(40) (a) J. H. Freed, *J. Chem. Phys.*, **66**, 4183 (1977); (b) *ibid.*, **41**, 2077 (1964).

where $a_{LKM,lm}$ are constants determined by the initial conditions. After a 90°_y pulse, $C'_{LKM,10}(0^+) \simeq \delta_{L0}\delta_{K0}\gamma_{\pi}B_0/kT \equiv \delta_{L0}\delta_{K0}\epsilon$ (B_0 is the magnitude of the applied field) while $C'_{LKM,00}(0^+) = C'_{LKM,20}(0^+) = 0$, implying that $a_{LKM,10} = \delta_{L0}\delta_{K0}\epsilon$, $a_{LKM,00} = a_{LKM,20} = 0$.

After the τ evolution time

$$C'_{LKM,10}(\tau) = \delta_{L0}\delta_{K0}\epsilon \exp[-(W_I + 2W_x)\tau] \quad (\text{A22})$$

leading to

$$C_{LKM,10}(\tau) = \epsilon \{\delta_{L0}\delta_{K0} \exp[-(W_I + 2W_x)\tau] - 1\} \quad (\text{A23})$$

In the text, where T_1 effects are omitted from the calculation, $C_{LKM,10}(\tau)$ is set equal to zero. If, instead, it is kept, its effect on the calculation comes in through the action of the second (i.e., 90°_x) pulse which transforms $C_{LKM,1\pm 1}(\tau)$ to

$$C_{LKM,1\pm 1}(\tau^+) = \mp \frac{1}{2} [C_{LKM,1-1}(\tau) - C_{LKM,11}(\tau)] - (i/2^{1/2})C_{LKM,10}(\tau) \quad (\text{A24})$$

so that $C_{LKM,1\pm 1}(\tau^+)$ is no longer the complex conjugate of $C_{LKM,1\pm 1}(\tau)$.

The T_1 correction in eq A24 for the two-pulse sequence is thus simple even for slow motions. In more complicated sequences, e.g., ones with three or more pulses, we must also consider the effect of the second pulse on $C_{LKM,10}(\tau)$. The second pulse can mix terms with nonzero L, K values into $C_{LKM,10}(\tau)$, which will then evolve during the subsequent evolution time (cf. eq A19-A21). The third pulse can then transfer these evolved nonzero L, K terms back into the corresponding off-diagonal elements where their effect will show up in measurements.

Appendix B

Effect of Inhomogeneous Broadening on the Quadrupole Echo. A purely homogeneous free induction decay (eq 26) written in terms of $C(\tau)$, O , Λ , and U is

$$C_i(\tau)_{\text{homogeneous}} \propto \sum_{jm} O_{ij} \exp[-(\text{Re } \Lambda_j + i \text{Im } \Lambda_j)\tau] O_{mj} U_m \quad (\text{B1})$$

$$= \sum_j a_{ij} \exp[-(\text{Re } \Lambda_j + i \text{Im } \Lambda_j)\tau] \quad (\text{B2})$$

with $a_{ij} = \sum_m O_{ij} O_{mj} U_m$. The corresponding CW spectrum is thus a superposition of complex Lorentzian line shapes having width = $\text{Re } \Lambda_j$ and frequency position = $\text{Im } \Lambda_j$. In the presence of inhomogeneous broadening, a range of $\text{Im } \Lambda_j$ values are present, call them $\text{Im } \Lambda_j + X_k$, and are distributed among the system molecules according to some weighting function $h(X_k)$. Equation B2 becomes

$$C_i(\tau) \propto \sum_k h(X_k) \sum_j a_{ij} \exp[-(\text{Re } \Lambda_j + i[\text{Im } \Lambda_j + X_k])\tau] \quad (\text{B3})$$

Following the second pulse

$$C_i(\tau^+) \propto \sum_k h(X_k) \sum_j a_{ij}^* \exp[-(\text{Re } \Lambda_j - i[\text{Im } \Lambda_j + X_k])\tau] \quad (\text{B4})$$

and during the second evolution time

$$C_p(\tau + \tau) \propto \left[\sum_{rj} a_{pr} a_{rj}^* \exp[-(\Lambda_r t + \Lambda_j^* \tau)] \right] \left\{ \sum_k h(X_k) \exp[-iX_k(t - \tau)] \right\} \quad (\text{B5})$$

where

$$a_{pr} = \sum_l O_{pr} O_{lr}$$

The sum over r, j in eq B5 is eq 29 written in terms of matrix elements of O and Λ . The single sum over k can be taken over to an integral in the limit that the X_k differ only infinitesimally. It then becomes the Fourier transform of the distribution function $h(X)$, i.e., $\tilde{h}(t - \tau)$.

Registry No. TMSI-d₉, 23726-00-3; HMB-d₁₈, 4342-40-9.

Excited and Ionic States of Polymers with Pendant Phenanthryl Groups in Solution. Model Systems for Photophysics in Phenanthrene Aggregates

Naoto Tamai, Hiroshi Masuhara,* and Noboru Mataga

Department of Chemistry, Faculty of Engineering Science, Osaka University, Toyonaka, Osaka 560, Japan (Received: March 3, 1983)

Using N_2 gas laser and picosecond Nd^{3+} :YAG laser photolysis systems, we measured the transient absorption spectra of 9-ethylphenanthrene (EPh), 1,3-di-(9-phenanthryl)propane (DPhP), poly[2-(9-phenanthryl)ethyl vinyl ether] (PPhEVE), and poly(9-vinylphenanthrene) (PVPh) in solution. The $S_n \leftarrow S_1$ absorption spectrum is almost common to the present compounds, indicating a very weak interchromophore interaction in the excited singlet state. The absorption spectrum of the triplet and cationic states changes from compound to compound, while the spectra of their anion radicals are identical. The triplet excitation and the positive hole can be stabilized easily by forming excimer and dimer cation, respectively, whose conformations are discussed in detail. In the case of polymer systems, plural dimer sites with different geometries exist, which is due to the stacking effect of chromophores. On the other hand, the negative charge is always trapped as a monomer anion. On the basis of the present results, the photophysics of phenanthrene aggregates is discussed.

Introduction

The study of primary photoprocesses such as energy migration, excimer formation, and charge separation is now one of the most important subjects in chemistry. Micellar solutions, microemulsions, vesicles, and membrane systems involving aromatic chromophores have been investigated by means of single photon counting and laser photolysis

measurements, and information on their excited-state dynamics is increasing quite rapidly. In these systems, the local concentration of aromatic chromophores is high, while their distribution is nonuniform. This will result in new kinds of dynamic behavior characteristics of molecular aggregates which may be observed by using time-resolved spectroscopy. In accordance with these developments,